Pharm Res (2011) 28:1973–1983
DOI 10.1007/s11095-011-0424-7

RESEARCH PAPER

Viscosity Analysis of High Concentration Bovine Serum Albumin Aqueous Solutions

Sandeep Yadav • Steven J. Shire • Devendra S. Kalonia

Received: 8 December 2010 / Accepted: 8 March 2011 / Published online: 14 April 2011

ABSTRACT

Purpose To understand the apparent inconsistency between the dilute and high concentration viscosity behavior of bovine serum albumin (BSA).

Method Zeta potential and molecular charge on BSA were determined from Electrophoretic mobility measurements. Second virial coefficient (B_{22}) and interaction parameter (k_D) obtained from static and dynamic light scattering, respectively, quantified intermolecular interactions. Rheology studies characterized viscoelasticity at high concentration. The dipole moment was calculated using Takashima's approximation for proton fluctuations over charged residues.

Results The effective isoelectric point of BSA was pH 4.95. In dilute solutions (≤ 40 mg/ml), the viscosity was minimal at the pI; at high concentrations, pH 5.0 solutions were most viscous. B_{22} and k_D showed intermolecular attractions at pH 5.0; repulsions dominated at other pHs. The attractive interactions led to a high storage modulus (G′) at pH 5.0.

Conclusion In dilute solutions, the electroviscous effect due to net charge governs the viscosity behavior; at high concentrations, the solution viscosity cannot be justified based on a single parameter. The net interplay of all intermolecular forces dictates viscosity behavior, wherein intermolecular attraction leads to a higher solution viscosity.

KEY WORDS dipole moment · high concentration viscosity · interaction parameter (k_D). · intermolecular interaction · protein charge · second virial coefficient (B_{22}) · zeta potential

Electronic supplementary material The online version of this article (doi:10.1007/s11095-011-0424-7) contains supplementary material, which is available to authorized users.

S. Yadav · D. S. Kalonia (✉)
Department of Pharmaceutical Sciences, University of Connecticut
Storrs, CT 06269, USA
e-mail: kalonia@uconn.edu

S. J. Shire
Late Stage Pharmaceutical Development
Genentech, Inc.
1 DNA Way
South San Francisco, CA 94080, USA

Present Address:
S. Yadav
Late Stage Pharmaceutical Development
Genentech, Inc.
South San Francisco, CA 94080, USA

INTRODUCTION

In 1956 Buzzel and Tanford published the viscosity of bovine serum albumin (BSA) and ribonuclease (RNAase) at various conditions of solution pH and ionic strengths (1,2). For the concentration range studied (~40–50 mg/ml) the solution viscosity showed a good correlation with the net charge-induced electroviscous effects. Due to the presence of electrical charge on the molecule, three kinds of contribution may affect the viscosity behavior. A 'primary effect' due to the resistance of the diffuse double layer surrounding the molecule, a 'secondary effect' due to the intermolecular repulsion between double layers and a 'tertiary effect' that may arise if the interparticle repulsion affects the shape of the macromolecule. These three are collectively known as the 'electroviscous effects' (3). When a charged particle moves through a medium comprising small ions, electrostatic interaction between the particle and the small ions results in a relative motion of the ions to the medium and consequently an additional viscous loss arises that contributes to the overall viscosity of the solution.

For BSA and RNAase solutions the slope of the reduced viscosity (η_{red}), i.e. the specific increment in viscosity as a

function of protein concentration (c), increased with an increase in molecular charge (1,2). An increase in solution ionic strength resulted in a decrease in the slope (η_{red} *versus* c), which finally attained a limiting value at high solution ionic strengths. The authors attributed this to the net molecular charge-induced primary and secondary electroviscous effects, which also correlated to some extent with Booth's theory (4) of anticipated increase in intrinsic viscosity [η] due to electroviscous effects (1,2).

The observed behavior suggests that the viscosity should increase with an increase in the molecular charge due to the additional resistance to flow offered by the electroviscous effects. It then follows that for a protein solution the viscosity should be minimal at the isoelectric point (pI), when the net molecular charge is zero, and should increase as the solution conditions are made more acidic or basic relative to the pI. For dilute protein solutions, this trend has generally been observed (5,6). Furthermore, for BSA solution, certain calculations have been presented using the original data in Tanford's work (2), which supports this argument (Fig. 1). The details of the calculation for Fig. 1 have been explained in the Discussion section of this work.

Recent studies on the viscosity behavior of high concentration protein solutions have shown an altogether different behavior. The viscosity for 120 mg/ml IgG_2 solution was observed to be highest at the pI (7), which is not in agreement with the net charge-induced electroviscous effects. Conversely, 130 mg/ml MAb-1 (IgG_1), with a measured pI of 7.8, showed the highest viscosity at pH 6.0 relative to other pHs studied (8,9). Salinas *et al.* suggested that the high viscosity observed for >50 mg/ml IgG_1 solution, at pH 6.0 was primarily due to electroviscous effects (10). On the contrary, Yadav *et al.* (11) did not observe a consistent interpretation of electroviscous effects to the viscosity behavior of four different MAbs. (11)

The dilute solution viscosity behavior of BSA, wherein the viscosity was observed to be minimal at the pI (Fig. 1), therefore, does not correlate with the recently published high concentration viscosity data on IgG molecules. The present study seeks to understand the apparent inconsistency between the dilute and high concentration viscosity behavior of protein solutions. In particular, the high concentration viscosity behavior of BSA solutions as well as the different factors that may be responsible for the observed behavior have been analyzed and discussed.

MATERIALS AND METHODS

Materials

The BSA (lyophilized, purity 99% and essentially fatty acid- and globulin-free (Catalogue number: A0281) was obtained from Sigma (St. Louis, MO). All other chemicals including acetic acid, sodium acetate, sodium chloride, histidine hydrochloride, monobasic and dibasic sodium phosphate, were obtained from Fisher Scientific (Fair Lawn, NJ). All chemicals used were reagent grade or higher. Deionized water equivalent to Milli-Q^{TM} grade was used to prepare all solutions. Millipore (Billerica, MA) Amicon Ultra centrifugation tubes with a molecular weight cut-off of 3 kD were obtained from Fisher Scientific. Quartz crystal discs with fundamental vibrating frequencies of 10 MHz and plated with gold electrodes on both sides were obtained from International Crystal Manufacturing Company (Oklahoma City, Oklahoma).

Methods

Acetic acid-sodium acetate (pH 4.0, 5.0), histidine hydrochloride (pH 6.0) and monobasic-dibasic sodium phosphate (pH 7.0 and 8.0) buffers were prepared with appropriate buffer concentrations so as to maintain the ionic strength at 15 mM at respective pHs, without the addition of any salt. The BSA

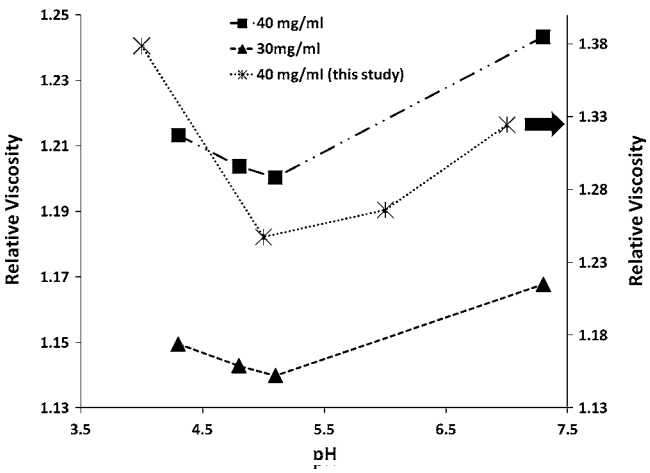

Fig. 1 The relative viscosity (η_{rel}) of BSA as a function of solution pH. The solid square and triangle (primary axis) are the η_{rel} calculated using Eq. 13 from the intercept [η] and slope, $k_H[\eta]^2$, reported by Tanford and Buzzel (2) at 10 mM ionic strength. The asterisk symbols (secondary axis) are the η_{rel} for 40 mg/ml BSA solution measured in this work.

solutions were buffer exchanged with the buffer of interest using Millipore Amicon Ultra centrifugation tubes. The concentrations of the sample were determined using UV spectrophotometry and an absorptivity of 0.667 $(mg/mL)^{-1}cm^{-1}$ at 280 nm (12) for 0.1% BSA solutions. The solution pH was checked for each dialyzed sample. Required concentrations were prepared by dilution with the respective buffer. To account for the Donnan effect in our experiments, the initial dialysis buffer pH was adjusted appropriately so that the final pH after dialysis matched the target pH and desired ionic strength. Additionally, at high concentration the protein itself will contribute to the ionic strength of the solution; however, the contribution of protein to the total ionic strength of solution is hard to quantify owing to a number of ionizable residues and their respective pKas, which may very well be different from the intrinsic pKas due to orientation and conformational placement of these residues in the folded state of the protein. For the purpose of this work, the final ionic strength of the solution will be specified as the contribution from buffer species at a particular pH and added salt, if any.

Further, an effort was made to reproduce only a part of Tanford's data (2) to ascertain a similar trend in dilute solution viscosity behavior arising due to electroviscous effects. For the purpose of these measurements, a similar procedure as described by Tanford *et al.* (2) was followed. The BSA was dissolved in triple distilled water and extensively exchanged against DI water using Amicon Ultra centrifugation tubes. Following this, the solution pH was adjusted using 0.1 N HCl or NaOH to the desired pH and final concentration of 40 mg/ml. The solutions were filtered through 0.22 μm Millipore Millex-W syringe filters and centrifuged at 6,740 *x g* for 5 min using an eppendorf minispin (Hamburg, Germany) centrifuge before making measurements.

Zeta Potential Analysis

Zeta potential (ξ) measurements were performed at 25 ± 0.1°C using a Malvern Zetasizer Nano Series (Worcestershire, UK) and DTS1060 clear disposable folded capillary cell. The methodology was kept consistent as detailed in a previous work.(11) The measured electrophoretic mobility was used to determine the ξ using Henry's equation:

$$U_E = \frac{2\varepsilon\xi f_1(\kappa a)}{3\eta} \tag{1}$$

where U_E is the electrophoretic mobility under the applied voltage, ε is the dielectric constant of the medium, η is the viscosity of the dispersant, ξ is the zeta potential in Volts and $f_1(\kappa a)$ is the Henry's function. The $f_1(\kappa a)$ is a function of the electrical double layer around the particle (13,14). At 15 mM solution ionic strength, the $f_1(\kappa a)$ value of 1.045 has been used to calculate the ξ.

Viscosity/Rheological Analysis

For dilute solutions (40 mg/ml BSA) a similar methodology as described by Tanford *et al.* was followed (2). The relative flow times were measured using a Cannon-Manning Semi-micro Size-25 capillary viscometer (Cannon Instrument Company, State College, PA). All the measurements were performed using the same viscometer at 25 ± 0.1°C. After each measurement the viscometer was cleaned immediately with hot sulfuric acid-dichromate solution, rinsed numerous times to remove all traces of the acid, and dried with filtered air. Flow times were recorded within $1/100^{th}$ of a second by means of electric timers. Four to five flow time measurements were made for each solution pH.

For high concentration solutions (250 mg/ml), the sample viscosities were measured using a VISCOlab 5000 viscometer system (Cambridge Viscosity, Medford, MA). A detailed procedure for measurement using VISCOlab 5000 was described in a previous work (11). The dynamic viscosities were determined at 25 ± 0.1°C by measuring the average travel time of the pistons calibrated over viscosity ranges 0.5–10.0 cP, 2.5–50 cP and 5–100 cP. All the samples were analyzed in triplicate. Note that the VISCOlab 5000 is a constant stress viscometer. However, the shear rate applied can be calculated by taking into account the applied stress, piston and annulus dimensions, the two way stroke and two way travel time of the piston (15,16). For the pistons employed for this study the shear rate ranged from 350 to 1,000 Hz. The BSA solutions, however, do not show a shear rate dependence up to a concentration of 404 mg/ml and 4,700 Hz (17). Before each measurement, the sample chamber was thoroughly cleaned with double-distilled water and dried with nitrogen.

The rheological properties of BSA were evaluated using an ultrasonic shear rheometer with quartz crystals vibrating at a fundamental frequency of 10 MHz. The theory and experimental procedure have been described previously (18). For non-Newtonian viscoelastic fluids, the solution storage (G′) and loss (G″) moduli and the complex viscosity (η*) can be related to the shift in electrical properties of the quartz crystal, i.e. series resistance (R_2) and reactance (X_2), by the following relationships (18):

$$G'(\omega) = \frac{R_2^2 - X_2^2}{A^2\rho_{Liq.}}, \tag{2}$$

$$G''(\omega) = \frac{2R_2X_2}{A^2\rho_{Liq}} \tag{3}$$

$$\eta^* = \left((G')^2 + (G'')^2\right)^{1/2}/\omega = G^*/\omega \tag{4}$$

where A is a crystal constant, ρ_{liq} is the liquid density, and ω is the quartz crystal frequency. In this study, 35-μL samples of the BSA solution were analyzed in triplicate.

Dynamic Light Scattering

DLS studies were conducted at 25±0.1°C using a Malvern Zetasizer Nano Series (Worcestershire, UK) as described previously (11). After buffer exchange, the protein solutions were filtered through 0.22 μm Millipore Millex-W syringe filters and centrifuged at 6,740 *x g* for 5 min using an eppendorf minispin (Hamburg, Germany) centrifuge. The Zetasizer Nano S utilizes a 632.8 nm Helium-Neon laser and analyzes scattered light at an angle of 173° using an avalanche photodiode. The DTS software was used to analyze the acquired correlogram (correlation function *versus* time) and obtain the mutual diffusion coefficient (D_m), which can be expressed as a function of solution concentration using the following equation (19):

$$D_m = D_s(1 + k_D c) \tag{5}$$

where D_s, is the self-diffusion coefficient (the value of D_m at infinite dilution as $c \rightarrow 0$) (20), k_D is the interaction parameter, and c is the concentration of the protein (g/ml). The value of D_s and k_D can be obtained, respectively, from the intercept and slope of a plot of D_m *vs.* c (Eq. 5). A positive value of the k_D corresponds to intermolecular repulsions, whereas a negative k_D signifies attractive interactions between molecules. The hydrodynamic radius (R_h) of the molecules can be estimated from the D_s using the Stokes-Einstein equation, $D_s = k_B T/6\pi\eta R_h$, where, k_B is the Boltzmann constant, T is the temperature in Kelvin, η is the solvent viscosity, i.e. $c \rightarrow 0$.

Static Light Scattering

SLS studies were conducted at 25±0.1°C using a Malvern Instruments (Worcestershire, UK) Zetasizer Nano S. Sample preparation steps were similar to that used for DLS. Samples were analyzed at 12 mg/ml and then sequentially diluted to lower concentrations. The average scattered intensity was obtained using the attenuation-corrected derived count rates from the Malvern Zetasizer (21). The Debye plots were then constructed from the average scattered intensities using the following equation:

$$\frac{KC}{R_\theta} = \frac{1}{M_w} + 2B_{22}c \text{ where the optical constant} \tag{6}$$

$$K = [2\pi n(dn/dc)]^2 / N_A \lambda_o^4 \tag{7}$$

M_w is the weight average molecular weight of the solute, c is the concentration in g/ml, λ_o is the wavelength of light used, N_A is Avogadro's number and dn/dc is the refractive index increment brought about by the solute under a given set of solution conditions.

Note that the Malvern Zetasizer Nano Series (Worcestershire, UK) uses an Avalanche Photodiode detector (APD) for recording the scattering intensity signal. Using the APD, both the SLS and DLS measurements can be performed simultaneously where the instrument measures the time-averaged scattered intensity for SLS and the time-dependent fluctuation in scattered intensity for DLS, by means of photon counting and photon correlation, respectively. However, the instrument uses an attenuator for recording the time-dependent fluctuation in scattered intensity while performing the DLS measurements, whereas there is no attenuation of the excess scattered intensity signal that reaches the detector while performing SLS measurements. This results in APD saturation in SLS measurements resulting in erroneous results. The correct average scattered intensity can, however, be determined from the attenuation-corrected count rates from the DLS measurements. A detailed procedure for such a correction to obtain correct SLS parameters using a Malvern Zetasizer is discussed elsewhere (21).

RESULTS

The asterisk symbol in Fig. 1 (secondary y-axis) shows the relative viscosity of a 40 mg/ml BSA solution measured using a capillary viscometer following a similar procedure as described by Tanford *et al.* (2) in his original work. At 40 mg/ml BSA at pH 5.0 showed a minimal viscosity compared to other pHs. The solid square and the triangles are 40 and 30 mg/ml, respectively, for BSA solution viscosities calculated from Tanford's work (2) and do not represent measurements made in this work. Further details on these calculations are elaborated in the Discussion section. Although Tanford's data already suggested a minimal viscosity around pH 5.0, the measurements were repeated to ensure that the trend observed in viscosity behavior, due to electroviscous effects in dilute solution, holds in general and was not an artifact of a different grade of BSA used previously in the study of Tanford *et al.* (2) The relative magnitudes of viscosity observed in the two studies are different and may be due to differences in purity of BSA obtained from different sources; however, the change in viscosity as a function of pH is consistent in the two studies.

Zeta Potential Measurements

Figure 2 shows the ξ of BSA molecules as a function of solution pH. The point of zero charge or the crossover point from a positive to negative potential, referred to as

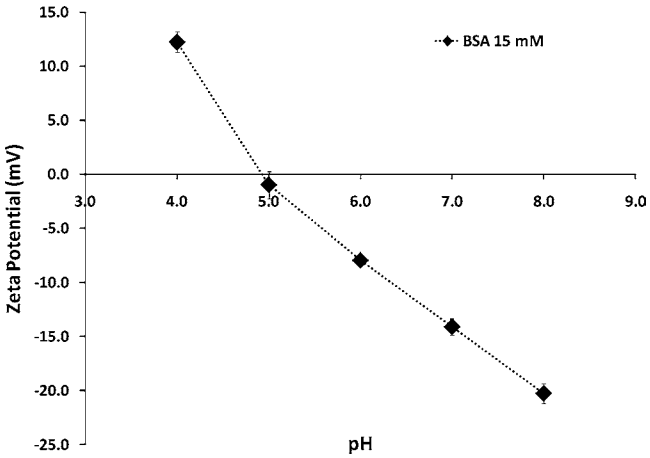

Fig. 2 Zeta potential of BSA molecules as a function of solution pH, 15 mM ionic strength at 25°C ± 0.1°C.

the isoelectric point (pI), was observed to be ~pH 4.95 (using linear interpolation), which is in good agreement with the reported values (22,23).

Since, the magnitudes of the observed ξ values are less than kT/e (i.e. 25.7 mV at 25°C), the net molecular charge, Z, can be obtained from a linear approximation of the Poisson-Boltzmann (PB) equation also known as the Debye-Huckel approximation (24):

$$z = \frac{4\pi\varepsilon a(1+\kappa a)\xi}{e} \tag{8}$$

where e is the electronic charge, a is the particle radius and κ^{-1} is the Debye length (thickness of the double layer). Note that the radius, a, in the Henry's and PB equations is different from the Stokes radius of the molecule. For the present charge calculations, the radius 'a' has been substituted by the hydrodynamic radius, 'R_h' calculated from D_s using the Stokes-Einstein equation, which results in an increase in charge estimates and brings them in line with calculated values (11,25). The ξ and Z estimated using Eq. 8 are compiled in Table I. At pH above and below pH 5.0, the BSA molecule carries a net positive or a negative charge, respectively, whereas at the pI (~pH 4.95), the net molecular charge is zero. The calculated net charge at different pH was in good agreement with the reported values of mean charge obtained from titration curves (23) (Supplementary Material Figure S1). The small variations are due to the difference in conditions of solution pH and ionic strength used in two studies (Supplementary Material Figure S1).

Low Shear Viscosity Measurements

Figure 3 shows the viscosity of 250 mg/ml BSA solution as a function of solution pH. The solution at pH 5.0 was observed to be most viscous in comparison with other pHs studied. The solution viscosity decreased with a change in solution pH towards acidic or basic side of pH 5.0.

Dynamic Light Scattering Measurements

The mutual diffusion coefficients (D_m) as a function of BSA concentration are plotted in Fig. 4. The parameters, k_D, D_s and R_h (Eq. 5), estimated from the slope and intercepts of linear fits in Fig. 4 are tabulated in Table II. BSA solutions at pH 4.0, 6.0 and 7.0 showed a positive slope and consequently a positive k_D, which indicate that the intermolecular interactions at these conditions are repulsive in nature. Conversely, pH 5.0 showed a negative k_D signifying the presence of intermolecular attractions.

Static Light Scattering Measurements

The Debye plots for BSA at different solution pH are shown in Figure S2. The B_{22} and molecular weight (M_w) obtained at different solution pHs are tabulated in Table II along with DLS results. Amongst all the pHs studied only pH 5.0 showed a negative B_{22} indicating the presence of attractive interaction between the molecules. All other pHs, including 4.0, 6.0 and 7.0, showed a positive B_{22} suggesting

Table I Zeta Potential (ξ), Net Molecular Charge (Z), Theoretical and Experimental Dipole Moment for BSA Molecule as a Function of pH

pH	Zeta potential (mV)	Experimental Charge [a]	Dipole moment	
			Theoretical [b]	Experimental [c]
4.0	+12.25 ± 0.96	6.96 ± 0.54	190	-
5.0	-0.99 ± 1.23	-0.57 ± 0.70	320	280
6.0	-7.96 ± 0.47	-4.52 ± 0.27	370	300
7.0	-14.13 ± 0.75	-8.02 ± 0.43	390	380
8.0	-20.30 ± 0.90	-11.02 ± 0.51	410	410

[a] Calculated from ξ measurement using the Debye-Huckel approximation of the Poisson Boltzmann equation (Eq. 8)

[b] Theoretical dipole moment from Supplementary Fig. S5

[c] Experimental values from Ref. (32)

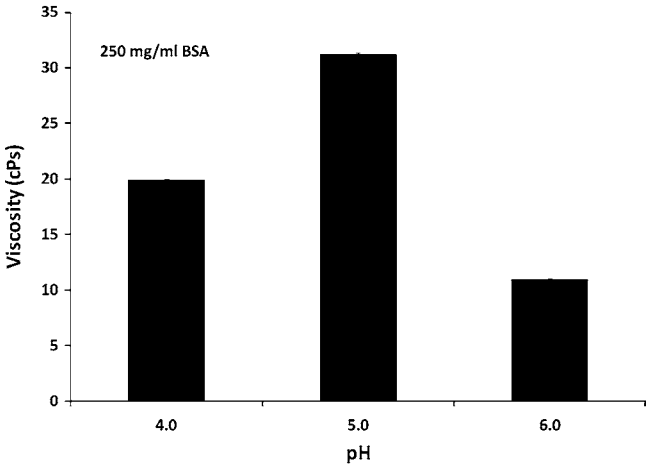

Fig. 3 The viscosity of 250 mg/ml BSA solution as a function of solution pH, 15 mM solution ionic strength, at 25°C ± 0.1°C.

intermolecular repulsions dominate at these pH conditions. The average M_w obtained (70.9 ± 3.1 kD) is higher than that of monomeric BSA determined by corrected amino acid sequence (66,430.3 kD) (26), and could result from the presence of about 3% dimers or higher oligomers. The osmotic second virial coefficient is principally affected by two contributions in the limit of infinite dilution, the (ideal) Donnan contribution to account for the electroneutrality in a multicomponent solution of polyelectrolyte, and the non-ideality contribution from protein-protein interactions (27,28). The Donnan contribution is particularly significant in low ionic strength solutions, wherein the Rayleigh ratio, R_θ, can be expressed as (27)

$$\frac{K}{R_\theta}\rho_2 = 1 + \frac{z^2}{2\rho_1}\rho_2 + \beta_{22}\rho_2 = 1 + 2B_{22}\rho_2 \qquad (9)$$

where ρ_1 and ρ_2 are the molar concentration of salt and protein component, respectively, z is the molecular charge, and the rest of the symbols carry the same meaning as in Eqs. 6 and 7. The $z^2/2\rho_1$ is the so-called Donnan term, and β_{22} is the non-ideal contribution from protein-protein interaction (27). To extract the contribution of intermolecular interaction, the Kc/R_θ adjusted for the Donnan contribution, $(1000c_2/M_w^2)$ $z^2/2\rho_1$ are plotted as a function of protein concentration in Supplementary Figure S2 and the contribution of the Donnan effect to overall B_{22} is compiled in Table II. The Donnan contribution is most significant at pH 4.0 and 7.0 since BSA carries a higher net charge at these pHs. A small Donnan contribution can be seen at pH 6.0 as well; however, pH 5.0 is least affected due to zero net charge. The intermolecular interactions after adjusting for the Donnan contribution are still attractive only for pH 5.0, whereas pH 4.0, 6.0 and 7.0 showed net repulsions.

High Frequency Rheology Measurements

Figure 5 shows the complex viscosity (η^*) for BSA solutions as a function of concentration. At concentrations above 150 mg/ml the η^*, data clearly reflect a pH-dependent viscosity behavior of BSA solution (Fig. 5). In concurrence with the low shear viscosity values, BSA solution at pH 5.0 showed higher viscosity (~ above 150 mg/ml) in comparison to other pH values. A distinctively steep increase in the η^* was observed above 150 mg/ml at pH 5.0. The non-newtonian complex viscosity (η^*) can be separated into an elastic and a viscous component, wherein the elastic or the storage component ($\eta' = G'/\omega$) serves as a measure of intermolecular interactions existing in the system (29).

A similar behavior is observed in solution G′ as a function of BSA concentration (Figure S3), wherein solution pH 5.0, above 150 mg/ml, showed the highest G′ magnitude and a sharp increase with concentration compared to other pHs. The rheological analysis at 10 MHz frequency is still in the linear response range, and the viscoelastic characteristics are discussed in detail in Figure S4. The characteristic G", G′, phase angle (δ) and relaxation times (τ) at 10 MHz for 250 mg/ml BSA solution at different pH are tabulated in Supplementary Material Table T1. The characteristic relaxation (τ) at 250 mg/ml BSA concentration is of the order of 10^{-9} seconds, which is well below the inverse frequency $\omega = 2\pi \times 10^{-7}$ sec. Figure 8 shows the solution G′ at 250 mg/ml BSA concentration as a function of pH. A high solution G′ at pH 5.0 indicates the presence of strong intermolecular interactions which confer on the protein solutions a solid-like behavior such that a significant fraction of the applied stress is stored during viscoelastic deformation.

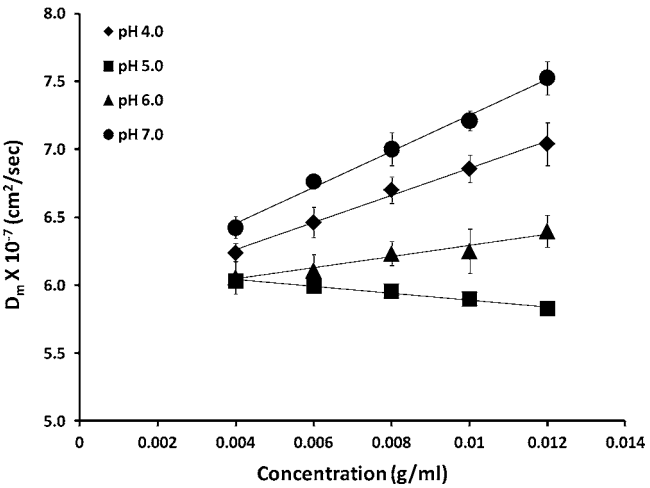

Fig. 4 Mutual diffusion coefficient (D_m) for BSA molecules as a function of concentration, at various pHs and 15 mM solution ionic strength. The lines are linear best fits with slope and intercept representing $D_s k_D$ and D_s (self-diffusion coefficient), respectively.

Table II Parameters Calculated from DLS and SLS Measurements with BSA Molecules at 15 mM Ionic Strength and 25 ± 0.1°C

Sample	D_sX10^{-7} (cm^2/sec) [a]	R_h (nm) [b]	k_D (ml/gm) [c]	B_{22} X10^{-4} (molml/gm^2)[d]	$Z^2/2\rho_1$X10^{-4} (molml/gm^2)[e]	β_{22} X10^{-4} (molml/gm^2) [f]	M_w (KDa) [g]
pH 4.0	5.86 ± 0.04	3.96 ± 0.03	17.04 ± 0.05	2.88 ± 0.67	1.80	1.08	69.1 ± 2.7
pH 5.0	6.14 ± 0.03	3.78 ± 0.02	-4.12 ± 0.03	-0.34 ± 0.19	0.01	-0.33	67.5 ± 2.4
pH 6.0	5.88 ± 0.11	3.95 ± 0.07	7.01 ± 0.14	1.31 ± 0.53	0.75	0.56	73.8 ± 2.9
pH 7.0	5.92 ± 0.03	3.92 ± 0.02	22.41 ± 0.04	3.38 ± 0.13	2.39	0.99	73.3 ± 0.7

[a] From the intercept of plots in Fig. 4,

[b] True Hydrodynamic diameter calculated at **c→0,**

[c] Slope (plots in Fig. 4) / D_s

[d,e] From the slope and intercept of linear fits in Debye Plots not adjusted for the Donnan contribution in Supplementary Figure S2,

[f] Donnan (ideal) contribution, (1,000/M_w^2) $z^2/4\rho_1$, to the B_{22}, Supplementary Figure S2

[g] Derived from the limiting slopes of quadratic fits in the limit of $C_2 = 0$. (Supplementary Figure S2)

Dipole Moment Calculations

The protein molecule consists of a number of charge residues on the surface and in the interior resulting in several dipoles and multipoles present simultaneously. The dipoles arise due to the asymmetrical charge distribution in protein molecules which can be determined experimentally using dielectric relaxation spectroscopy. Oncley and coworkers obtained experimental results for the dipole moment for several proteins. Except for β-Lactoglobulin with $\mu =$ 700 D, the dipole moment for other proteins (human serum albumin, horse hemoglobin, ovalbumin) was of the order of 200–400 D (30). However, note that it just requires a single pair of charge residues to be separated over an average molecular diameter of 70Å to result in a dipole moment of 329 D. Another possibility was proposed by Kirkwood and Shumaker, wherein the fluctuation of mobile protons on surface residues gives rise to a non-vanishing square dipole moment ($\Delta\mu^2$), the magnitude of which is given by the following equation (31):

$$\Delta\mu^2 = e^2 f^2 b_o^2 \sum_{\alpha} \frac{\nu_\alpha}{2 + K_\alpha/[H^+] + [H^+]/K_\alpha} \tag{10}$$

where,

$$f^2 = \frac{\sigma^{\frac{3}{4}}}{4} \frac{(\sigma^2+2)\sqrt{\sigma^2-1} + \sigma^2(\sigma^2+4)\sec^{-1}\sigma}{\sigma^2\sqrt{\sigma^2-1} + \sigma^4\sec^{-1}\sigma} \tag{11}$$

and $\sigma = a/b$, $b_0 = (ab^2)^{1/3}$, where σ is the axial ratio, b_0 is the radius of the equivalent sphere and ν_α is the equivalent number of titratable groups of the type α in the molecule. Assuming that the charge distribution is symmetrical to result in an average dipole moment $\overline{\mu} = 0$, the authors (31) calculated the dipole moment contribution solely due to proton fluctuations and found that the $\Delta\mu$ (dipole moment fluctuations) values were of the order of experimental values in Oncley's work (30). This indicates that the experimentally observed dipole moment for studied proteins could just be accounted for by charge fluctuations, and the molecules do not necessarily require possessing an asymmetrical distribution of surface residues or the mean dipole moment.

In a later work, Takashima correlated the fluctuations of the protons with the thermodynamic fluctuations to come up with the following equation for induced dipole moment associated with charge fluctuation (32):

$$\Delta\mu^2 = \left(e^2 f^2 b_o^2\right) kT \sum_i \sigma_i [K_i/([H^+](1 + K_i/[H^+]))] \tag{12}$$

where k is the Boltzmann constant; T is temperature in Kelvin; f, e, and b_o have the same meaning as in Eqs. 10 and 11; and σ_i is the charge density per unit area. The

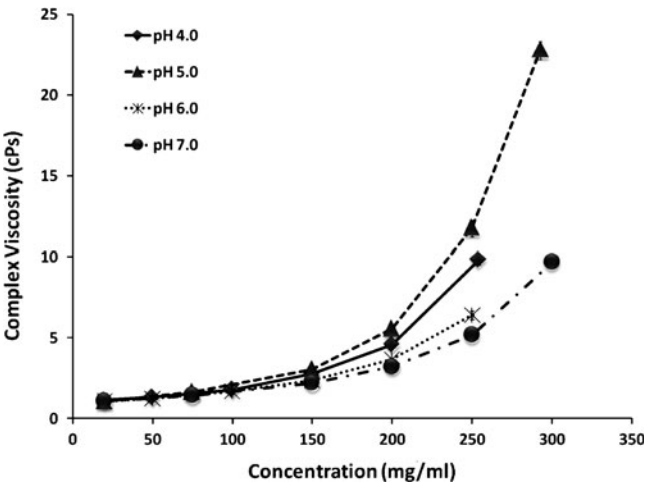

Fig. 5 Solution complex viscosity (η^*) as a function of BSA concentration at various pHs and 15 mM ionic strength, measured using ultrasonic shear rheometer at 10 MHz frequency.

theoretically calculated dipole moment using Eq. 12 showed a good agreement with the experimentally measured dipole moments for BSA and ovalbumin (32).

Supplementary Figure S5 shows the dipole moment for BSA as a function of pH, calculated using Eq. 12. In Figure S5, no new results are obtained, and the data only reproduce the dipole moment calculations performed by Takshima using the updated BSA amino acid sequence reported by Hirayama *et al.* (26). The theoretically calculated (Fig. S5) and experimentally measured dipole moments (from Takashima's work) (32) as a function of solution pH are tabulated along with the molecular charge data in Table I. The dipole moment of BSA increased from ~190 Debye at pH 4.0 to ~ 320 Debye at pH 5.0. However, over pH 6.0 to 8.0, the magnitude of the dipole showed a gradual increase from ~ 370 Debye at pH 6.0 to 400 Debye at pH 8.0.

DISCUSSION

Tanford and Buzzel (2) in their original work tabulated the values of the extrapolated intrinsic viscosity, $[\eta]$, and the slopes for reduced viscosity *versus* concentration plots for BSA solutions at various solution pHs and ionic strength. The concentration dependence of reduced viscosity (η_{red}) is often expressed in terms of the relation (33):

$$\eta_{red} = \eta_{sp}/c = [\eta] + k_H[\eta]^2 c \tag{13}$$

where c is the concentration in g/ml, k_H is the Huggins coefficient, $[\eta]$ is the intrinsic viscosity in ml/g, and η_{sp} is the specific viscosity defined as $\eta_{sp} = (\eta - \eta_o)/\eta_o = \eta_{rel} - 1$, where η and η_{o} are the solution and solvent viscosity, respectively. $\eta_{\mathrm{rel}} = \eta/\eta_{\mathrm{o}}$ denotes the relative viscosity of a solution. A linear extrapolation of η_{red} *versus* c to zero concentration ($c \rightarrow 0$) yields $[\eta]$ as the intercept and $k_{\mathrm{H}}[\eta]^2$ as the slope. Given the values of intercept, $[\eta]$, and slope, $k_{\mathrm{H}}[\eta]^2$, it is possible to calculate the relative viscosity, η_{rel}, or vice versa. Figure 1 shows the relative viscosity for BSA solutions calculated using the $[\eta]$ and slope values reported at 10 mM solution ionic strength in Tanford's work (2). Since the authors (2) reported that the isoionic pH of BSA in water was 5.0, which increased to 5.6 at 500 mM chloride concentration, the pH at 10 mM chloride concentration was assumed to be pH 5.1. The η_{rel} data of BSA under dilute conditions (30 and 40 mg/ml) clearly indicate that the viscosity is minimal near the pI (Fig. 1: η data at pH 4.8 or pH 5.1). This is further substantiated by the viscosity of 40 mg/ml BSA solution measured in this work, which consistently showed a lower viscosity at solution pH 5.0. ξ measurements showed that the net molecular charge is nearly zero (Table I) at this pH. As the BSA molecule acquires a net positive (pH=4.3) or a net negative charge (pH=7.3), the associated electroviscous effects led to an increase in solution viscosity (Fig. 1).

However, this is true only up to a limited concentration range, because at high concentrations (> 150 mg/ml), pH 5.0 was observed to be most viscoelastic relative to all other pHs studied (Figs. 3 and 5). For a clear distinction, the dilute (40 mg/ml) and high concentration (250 mg/ml) viscosity data as a function of solution pH are plotted in Fig. 6. Unlike 40 mg/ml, the viscosity at 250 mg/ml is highest at pH 5.0 and drops with a change in solution pH to either the acidic or the basic side of pH 5.0. The high viscosity observed at the pI, for >150 mg/ml BSA solution (Figs. 5 and 6) cannot be explained based on net charge-induced primary or secondary electroviscous effects and needs further explanation.

At high concentrations solutions, the molecules are fairly close to each other, and thus intermolecular potentials other than just electroviscous effects also become important. Accurate calculation of these interaction energies between protein molecules is, however, complicated, due to the complex geometry of these molecules as well as the angular dependence of interactions due to the uneven surface charge distribution. Nevertheless, the main contribution towards intermolecular interaction energy comes from electrostatic, Van der Waals, and excluded volume interactions. In addition to these non-specific forces, there could also be specific interactions governed by local geometry and the high degree of complimentarity between molecules besides the protein-solvent and hydrogen bonding interactions associated with protein solutions.

Extending the colloidal interaction theory to protein systems, the potential of mean force, W_{12}, between molecules can then be expressed as sum of mean force contributors (34,35):

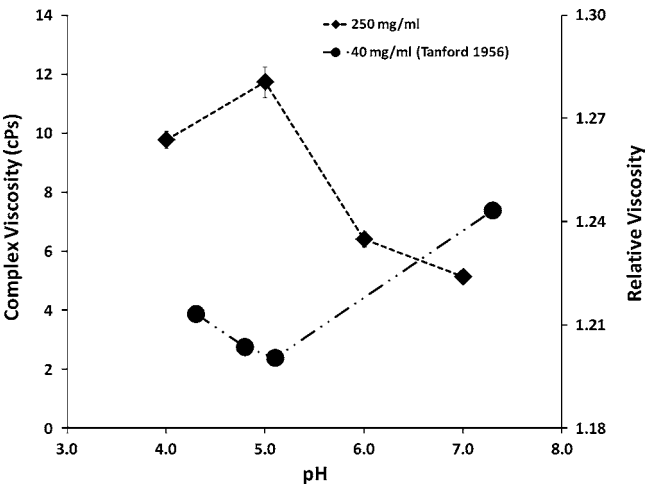

Fig. 6 The solution complex viscosity (η^*) for 250 mg/ml BSA solution (left axis) and the relative viscosity (η_{rel}) for 40 mg/ml BSA solution (right axis) as a function of solution pH.

$$W_{12}(r) = W_{HS}(r) + W_{q-q}(r) + W_{q-\mu}(r) + W_{q-i\mu}(r) + W_{\mu-\mu}(r) + W_{\mu-i\mu}(r) + W_d(r) \quad (14)$$

where W_{HS} is the excluded volume (hard sphere) contribution, $W_{q\text{-}q}$ is the charge-charge interaction, $W_{q\text{-}\mu}$ is the charge-dipole interaction, $W_{\mu\text{-}\mu}$ is dipole-dipole interaction, $W_{q\text{-}i\mu}$ is the charge-induced dipole interaction, $W_{\mu\text{-}i\mu}$ is dipole-induced dipole interaction, and W_d is the dispersion/Van der Waals contribution to intermolecular interaction energy. Only the first two terms in Eq. 14 constitute repulsive forces. All other terms represent attractive contribution to the intermolecular energy, where charge-dipole and charge-induced dipole express much larger influence to intermolecular interactions as compared to dipole-dipole and dipole-induced dipole interaction energy. The conventional measures of intermolecular interactions, such as second virial coefficient (B_{22}) or interaction parameter (k_D), essentially overlay the protein-solvent interactions and represent a measure of protein-protein interaction over protein-solvent interactions.

The excluded volume, $W_{HS}(r)$, contribution depends on the size and shape of the protein molecule. Hydrodynamic parameters such as intrinsic viscosity measurements can give information about the effective molecular size. The excluded volume can then be approximated as 4 times the volume of the molecule (36).

The charge-charge electrostatic repulsion, $W_{q\text{-}q}(r)$, is the leading term when the molecules carry a high net charge and is inversely related to the square of distance between molecules (34,35,37). This contribution from charge-charge repulsions would decrease with decrease in net molecular charge and should become zero at the pI. Whereas at or near the pI the contribution from electrostatic charge-dipole, dipole-dipole and long range Van der Waals attractive interactions would increase over protein solvent interactions. The dipole moment contribution will be lower at pH < 3.0 and at pH > 10.0 due to lack of negatively and positively charged residues, respectively. The next important intermolecular force is the Van der Waals interactions (38). When dealing with macromolecules, it is often the case that this interaction force is not significant unless the separation distance is small as compared to the molecular radii. Thus, the Van der Waals attractions are present at both short and long distance, but it might be too weak to be significant over long distances (39). The force, however, may dominate electrostatic repulsion at separations of the order of a few angstroms, where the molecules may orient to present geometrically complimentary surface (40). The observed viscosity behavior of BSA molecules, as well as the intermolecular interactions (B_{22} and k_D) as a function of solution pH, can be explained based on the interplay of these forces.

The first contribution, as mentioned before, is the excluded volume, $W_{HS}(r)$, arising due to the effective molecular volume and the solute volume fraction in solution. For concentrated non-interacting spherical particles, where the primary contribution to solution viscosity is from the excluded volume, the viscosity behavior can be approximated by the Ross and Minton equation (41):

$$\eta = \eta_o \exp\left[[\eta]c \Big/ \left(1 - \frac{k}{\nu}[\eta]c\right)\right] \quad (15)$$

where $[\eta]$ is the intrinsic viscosity in ml/g, k denotes the self-crowding factor, c is the concentration in g/ml, and ν is the Simha shape parameter (42). Equation 15 takes into account only the first-order interaction parameter, i.e. crowding effect (k) with an increase in solute concentration. Molecular crowding is essentially a consequence of the excluded volume effect, i.e. the solution volume excluded/not available to a molecule, strictly because of steric reasons, due to the introduction/presence of another molecule in solution. The Ross and Minton equation (Eq. 15), therefore, enables one to assess the impact of effective molecular volume on solution viscosity.

To elucidate the influence of molecular crowding/excluded volume on the viscosity behavior of BSA at various solution pHs, the $[\eta]$ values reported in Tanford's work at pH 4.3, 4.8, 5.1 and 7.3 and 10 mM ionic strength were used (2). Based on previous observations on hemoglobin (Hb) solutions ($k/\nu = 0.40$) (41) and IgG_1 solutions ($k/\nu =$ 0.37 to 0.49) (11,43) a reasonable value of $k/\nu = 0.45$ was assumed for the calculations. The theoretically calculated viscosity behavior (using Eq. 15) as a function of BSA concentration is plotted in Fig. 7. The analysis suggests that a difference in molecular size can result in significant viscosity difference at high concentration. However, if only the excluded volume effect was to govern the viscosity behavior, solution pH 7.3 should have been most viscous, and pH 5.0 should have been the least viscous of all, which do not correlate with observed viscosity behavior. It must be noted that the above calculations are only rough estimates considering the assumed value of k/ν approximated over the whole concentration range. However, qualitatively it gives a good approximation of the outcome of effective molecular volume on the viscosity behavior. Nonetheless, the analysis suggests that forces other than excluded volume need to be considered in order to explain the solution behavior of BSA at high concentrations.

The overall solution behavior at high concentration is governed by the net interplay of all the forces and cannot be justified based on a single parameter such as, the net charge or the net dipole (Fig. S5, Table I) or the volume exclusion effects (Fig. 7). The viscosity behavior in dilute and high concentration solution is more consistent with the

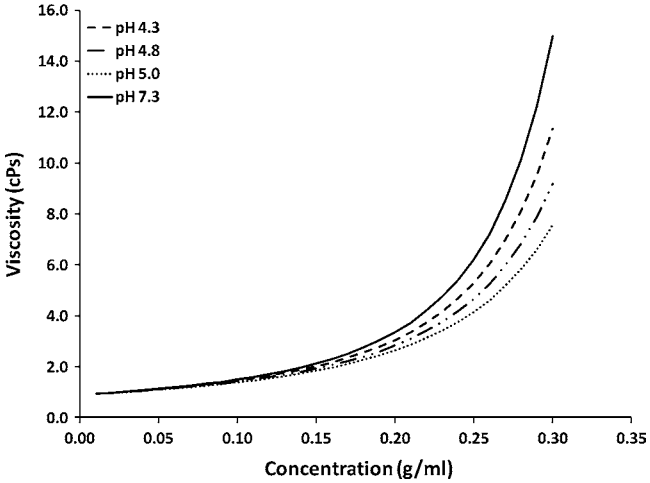

Fig. 7 The theoretical estimated viscosity *versus* concentration profile for BSA solution at various solution pH, calculated using Eq. 15. pH 4.3 dash line (– – –); pH 4.8 dash and dotted line (– · · –); pH 5.0 dotted line (·····); pH 7.3 solid line (—). The *k*/*v* was assumed to be 0.45 and [η] at various solution pHs were obtained from reference (2).

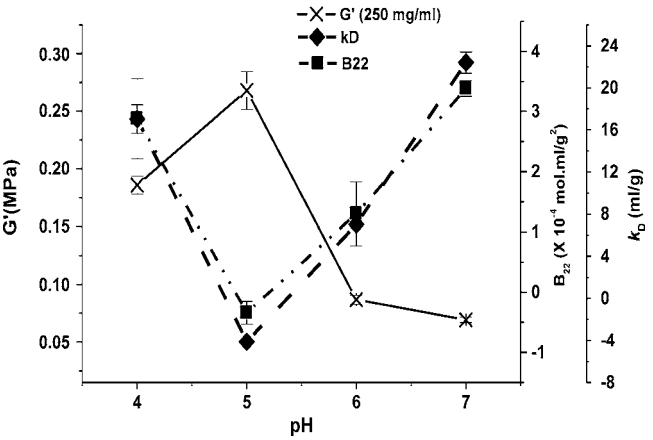

Fig. 8 The solution G′ for 250 mg/ml BSA (left axis) and dilute solution intermolecular interaction parameters, second virial coefficient, B_{22}, (right axis) and interaction parameter, k_D (right axis) as a function of solution pH and 15 mM solution ionic strength.

net interplay of intermolecular interactions in the system. Figure 8 shows the dilute solution interaction parameters, i.e. B_{22} and k_D along with solution G′ for 250 mg/ml BSA as a function of pH. The experimental results (ξ, χ, B_{22} and k_D) were observed to be fairly consistent with each other. The absolute molecular charge (|Z|) on BSA was highest for pH 8.0 followed by pH 7.0>pH 4.0>pH 6.0. The charge-induced repulsions and consequently positive B_{22}, and k_D at pH 8.0 was >pH 7.0>pH 4.0>pH 6.0. At pH 5.0, where the net molecular charge and, therefore, the charge-induced repulsions are minimal, intermolecular attraction dominates as evident from a negative magnitude of B_{22} and k_D. The solution G′ exhibits a maximum at pH 5.0, wherein the intermolecular interactions are attractive in nature (negative B_{22} and k_D). As the molecule acquires a net charge away from the pI, the repulsive interactions dominate and the G′ decreases. At high concentrations or short inter-separation distances, the presence of intermolecular attractions result in low energy molecular alignments leading to long-range order in the solutions. This results in a higher resistance to momentum transfer and an increase in relaxation time, (Supplementary Material Table T1) in the presence of attractive interactions as compared to intermolecular repulsion. Since the rigidity conferred to the system due to attractive interactions will be higher as compared to the intermolecular repulsions, attractive interactions result in higher solution G′. The energy dissipated during viscoelastic deformation will need to overcome this long-range order or rigidity in the system to induce flow, which therefore results in a higher solution viscoelasticity and G′, and hence viscosity at pH 5.0 in comparison with other pHs (Figs. 7, 8, 250 mg/ml BSA solution).

SUMMARY AND CONCLUSIONS

At low concentrations (~40 mg/ml) the electroviscous effects dominates, and the viscosity of BSA solutions is governed primarily by the net charge on the molecule. Thus, in dilute solutions, the viscosity was minimal at the pI (~ 4.95), where the net molecular charge is zero, and was higher at pHs away from the pI due to an increase in the net molecular charge. Although the attractive interactions are present even in dilute solutions, these are too weak to be of significance. The repulsive intermolecular potentials, being columbic, are long ranged and are thus influential even in dilute solutions or large inter-separation distance. Hence, the repulsive electroviscous effect leads to a viscosity increase at pHs away from the pI. (Fig. 7, 40 mg/ml BSA solution). Conversely, at high concentrations (> 200 mg/ml), the intermolecular separation distance decreases, resulting in an increased contribution from the short-range attractive interactions. These short-range attractive interactions dominate at the pI, where the net molecular charge and therefore the charge-induced repulsions are minimal. Consequently, at the pI the dominance of attractive interactions increases the self-associating behavior of BSA molecules, thereby resulting in a transient network and increased resistance to flow leading to a high solution viscosity.

ACKNOWLEDGMENTS

The authors acknowledge generous financial support from Genentech, Inc. Gerald J. Jackson Memorial Foundation at University of Connecticut in the form of student fellowship is also greatly acknowledged.

REFERENCES

1. Buzzell JG, Tanford C. The effect of charge and ionic strength on the viscosity of ribonuclease. J Phys Chem. 1956;60:1204–7.
2. Tanford C, Buzzell JG. The viscosity of aqueous solutions of bovine serum albumin between pH 4.3 and 10.5. J Phys Chem. 1956;60:225–31.
3. Harding SE. Dilute solution viscometry of food biopolymers. In: Hill SE, Ledward DA, Mitchell JR, editors. Functional properties of food macromolecules. Gaithersburg: Aspen; 1998. p. 77–142.
4. Booth F. The electroviscous effect for suspensions of solid spherical particles. Proc Roy Soc (London). 1950;A203:533–51.
5. Bull HB. Electroviscous effect in egg albumin solutions. Trans Faraday Soc. 1940;36:80–4.
6. Komatsubara M, Suzuki K, Nakajima H, Wada Y. Electroviscous effect of lysozyme in aqueous solutions. Biopolymers. 1973;12:1741–6.
7. Saluja A, Badkar AV, Zeng DL, Nema S, Kalonia DS. Application of high-frequency rheology measurements for analyzing protein-protein interactions in high protein concentration solutions using a model monoclonal antibody (IgG_2). J Pharm Sci. 2006;95:1967–83.
8. Liu J, Nguyen MDH, Andya JD, Shire SJ. Reversible self-association increases the viscosity of a concentrated monoclonal antibody in aqueous solution. J Pharm Sci. 2005;94:1928–40.
9. Yadav S, Liu J, Shire SJ, Kalonia DS. Specific interactions in high concentration antibody solutions resulting in high viscosity. J Pharm Sci. 2010;99:1152–68.
10. Salinas BA, Sathish HA, Bishop SM, Harn N, Carpenter JF, Randolph TW. Understanding and modulating opalescence and viscosity in a monoclonal antibody formulation. J Pharm Sci. 2009;99:82–93.
11. Yadav S, Shire SJ, Kalonia DS. Factors affecting the viscosity in high concentration solutions of different monoclonal antibodies. J Pharm Sci. 2010;99:4812–29.
12. Fasman GD. CRC practical handbook of biochemistry and molecular biology: proteins. Boca Raton, FL: CRC; 1976.
13. Hunter RJ. The calculation of zeta potential. In: Ottewilland RH, Rowell RL, editors. Zeta potential in colloid science principles and applications. New York: Academic; 1981. p. 59–124.
14. Delgado AV, Gonzalez-Caballero F, Hunter RJ, Koopal LK, Lyklema J. Measurement and interpretation of electrokinetic phenomena. J Colloid Interface Sci. 2007;309:194–224.
15. High Speed, Small Sample Rheometric Screening using Cambridge Viscometer. http://www.cambridgeviscosity.com/articles/RheometricFluidScreeningTechnique.pdf.
16. Estimating Shear Rate in CVI Viscometer. Technical Note: 03-002b.
17. Application Note: Viscosity measurement of a model protein solution of BSA. http://www.rheosense.com/images/ApplicationsArticles/APP-04_Viscosity-of-BSA-in-PBS.pdf.
18. A. Saluja and D.S. Kalonia. Measurement of fluid viscosity at microliter volumes using quartz impedance analysis. AAPS PharmSciTech. 5:Article 47 (2004).
19. Brown W, Nicolai T. Dynamic light scattering: the method and some applications. New York: Oxford University Press; 1993.
20. Veldkamp WB, Votano JR. Effects of intermolecular interaction on protein diffusion in solution. J Phys Chem. 1976;80:2794–801.
21. S. Yadav, T. Scherer, M., S.J. Shire, and D.S. Kalonia. Use of Dynamic Light Scattering to determine Second Virial Coefficient in Semi-dilute Concentration Regime. Anal Biochem: doi:10.1016/j.ab.2010.1012.1014 (2010).
22. Carterand DC, Ho JX. Structure of serum albumin. Adv Protein Chem. 1994;45:153–203.
23. Tanford C, Swanson SA, Shore WS. Hydrogen-ion equilibria of bovine serum albumin. J Am Chem Soc. 1955;77:6414–21.
24. Hunter RJ. Charge and potential distribution at interface. In: Ottewilland RH, Rowell RL, editors. Zeta potential in colloid science principles and application. New York: Academic; 1981. p. 11–58.
25. Durant JA, Chen C, Laue TM, Moody TP, Allison SA. Use of T4 lysozyme charge mutants to examine electrophoretic models. Biophys Chem. 2002;101–102:593–609.
26. Hirayama K, Akashi S, Furuya M, Fukuhara K. Rapid confirmation and revision of the primary structure of bovine serum albumin by ESIMS and Frit-FAB LC/MS. Biochem Biophys Res Commun. 1990;173:639–46.
27. Asthagiri D, Paliwal A, Abras D, Lenhoff AM, Paulaitis ME. A consistent experimental and modeling approach to light-scattering studies of protein-protein interactions in solution. Biophys J. 2005;88:3300–9.
28. Paliwal A, Asthagiri D, Abras D, Lenhoff AM, Paulaitis ME. Light-scattering studies of protein solutions: Role of hydration in weak protein-protein interactions. Biophys J. 2005;89:1564–73.
29. Saluja A, Badkar AV, Zeng DL, Nema S, Kalonia DS. Ultrasonic storage modulus as a novel parameter for analyzing protein-protein interactions in high protein concentration solutions: correlation with static and dynamic light scattering measurements. Biophys J. 2007;92:234–44.
30. Cohn EJ, Edsall JT. The Electric Moments and the Relaxation Times of Proteins as Measured from their Influence upon the Dielectric Constants of Solutions. In: Cohnand EJ, Edsall JT, editors. Proteins, amino acids and peptides as ions and dipolar ions. New York: Reinhold; 1943. p. 543–68.
31. Kirkwood JG, Shumaker JB. The influence of dipole moment fluctuations on the dielectric increment of proteins in solution. Proc Natl Acad Sci. 1952;38:855–62.
32. Takashima S. Proton fluctuation in protein. Experimental study of the Kirkwood-Shumaker theory. J Phys Chem. 1965;69:2281–6.
33. Huggins ML. The viscosity of dilute solutions of long-chain molecules. IV. Dependence on concentration. J Am Chem Soc. 1942;64:2716–8.
34. Haynes CA, Tamura K, Korfer HR, Blanch HW, Prausnitz JM. Thermodynamic properties of aqueous.alpha.-chymotrypsin solution from membrane osmometry measurements. J Phys Chem. 1992;96:905–12.
35. Vilker VL, Colton CK, Smith KA. The osmotic pressure of concentrated protein solutions: effect of concentration and ph in saline solutions of bovine serum albumin. J Colloid Interface Sci. 1981;79:548–66.
36. Hiemenz and P. C. Polymer Chemistry: The Basic Concepts, CRC Press, 1984.
37. Coen CJ, Newman J, Blanch HW, Prausnitz JM. Electrostatic protein-protein interactions: comparison of point-dipole and finite-length dipole potentials of mean force. J Colloid Interface Sci. 1996;177:276–9.
38. Jacob I. Intermolecular and surface forces. San Diego: Academic; 1992.
39. R.J. Hunter. Zeta Potential in Colloid Science Principles and Application, Academic Press Inc. New York 10003, 1981.
40. Roth CM, Neal BL, Lenhoff AM. Van der Waals interactions involving proteins. Biophys J. 1996;70:977–87.
41. Ross PD, Minton AP. Hard quasispherical model for the viscosity of hemoglobin solutions. Biochem Biophys Res Commun. 1977;76:971–6.
42. Mehl JW, Oncley JL, Simha R. Viscosity and the shape of protein molecules. Science. 1940;92:132–3.
43. Kanai S, Liu J, Patapoff TW, Shire SJ. Reversible self-association of a concentrated monoclonal antibody solution mediated by Fab-Fab interaction that impacts solution viscosity. J Pharm Sci. 2008;97:4219–27.